Journal of Materials Chemistry A

Accepted Manuscript

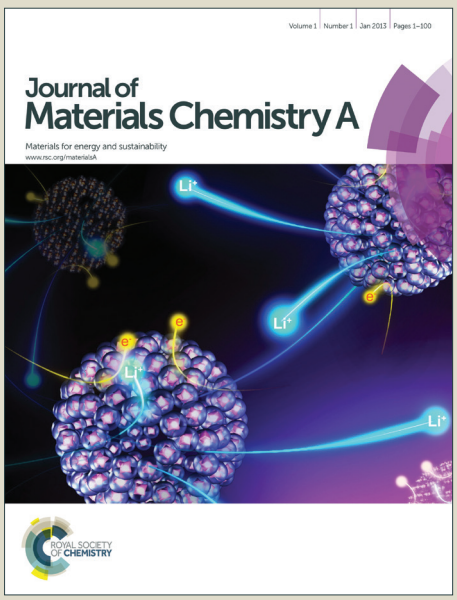

ROYAL SOCIETY OF CHEMISTRY

www.rsc.org/materialsA

Journal of Materials Chemistry A RSCPublishing

ARTICLE

Enhancement of photovoltaic properties of $CH_3NH_3PbBr_3$ heterojunction solar cells by modifying mesoporous TiO_2 surface with carboxyl groups

Cite this: DOI: 10.1039/xoxxooooox

Received ooth January 2012,
Accepted ooth January 2012

DOI: 10.1039/xoxxooooox

www.rsc.org/

Hyun Bin Kim,[a] Iseul Im,[a] Yeomin Yoon,[a] Sang Do Sung,[a] Eunji Kim,[b] Jeongho Kim,*[b] and Wan In Lee*[a]

In a new heterojunction solar cell employing $CH_3NH_3PbBr_3$ ($MAPbBr_3$) as light absorber, we found that the introduction of a carboxylate monolayer on the mesoporous TiO_2 surfaces significantly enhances J_{SC} as well as V_{OC}. In particular, the presence of a bromoacetate monolayer at the interface of TiO_2/$MAPbBr_3$ remarkably increases the photovoltaic conversion efficiency (PCE) from 2.65% to 5.57% with J_{SC} of 5.411 mA/cm^2, V_{OC} of 1.372 V, and FF of 0.75. Time-resolved photoluminescence measurements indicate that presence of the interfacial carboxylate groups expedites electron injection from $MAPbBr_3$ to TiO_2. Furthermore, according to pulsed light-induced transient measurements (PLITM) of photocurrent analysis, the lifetime of photoinjected electrons (τ_e) in TiO_2 conduction band (CB) significantly increases with the passivation of the interface, implying the suppression of charge recombination as well.

Introduction

Solid-state perovskite solar cells that utilize methylammonium lead halide ($CH_3NH_3PbX_3$, X=I, Br or Cl) as light absorber have attracted extensive interest as next-generation photovoltaics, ever since the first report in 2012.[1,2] In the perovskite solar cells, hole-transporting material (HTM) is commonly employed to mediate the transfer of holes generated in the perovskite light absorber into the counter electrode (CE). Presently, perovskite solar cells with photovoltaic conversion efficiencies (PCEs) approaching to 20% have been reported (currently 20.1% certified).[3-5]

Heterojunction solar cells (HSCs) without employing HTM have also been investigated as a new type of solar cells. In constructing HSC, mainly PbS-based quantum dots have been applied as light absorber,[6-8] and recently perovskite materials such as $CH_3NH_3PbI_3$ ($MAPbI_3$) were also utilized.[9-14] In the perovskite-based HSC, the highest PCE thus far reported was 10.49%,[14] which is considerably lower than that of conventional perovskite solar cells employing HTM such as spiro-OMETAD. Nonetheless, the HSC has several advantages in comparison with the conventional perovskite solar cells. First of all, the HSC devices can be prepared quite simply with low fabrication cost, because HTM layer, the most expensive component, is not employed. In addition, the HSC devices do not require the compact TiO_2 layer that plays the role of blocking the direct contact between TCO and HTM.[15,16] Furthermore, higher open circuit voltage (V_{OC}) might be achieved because the voltage drop, which is estimated to be the energy difference between the valence band (VB) of light absorber and the HOMO of HTM, can be avoided.

$CH_3NH_3PbBr_3$ ($MAPbBr_3$) has often been used as light absorber of perovskite solar cells,[17-22] but it has never been applied to HSC to our knowledge. The highest PCE reported for a perovskite solar cell adopting $MAPbBr_3$ is only 6.7% thus far,[20] and theoretical maximum current is estimated to be only 12.5 mA/cm^2 under AM 1.5G. Such low PCE can be ascribed to the wide band gap (2.2 eV) of $MAPbBr_3$, thus preventing the absorption of photons at wavelengths longer than 550 nm. In contrast, however, $MAPbBr_3$ perovskite solar cells can provide ultrahigh V_{OC} larger than 1.3 eV, which can be applied as an energy source for several photoelectrochemical reactions. For instance, its high V_{OC} is suitable for a bias voltage boosting photoelectrochemical reactions including water-splitting reactions or CO_2 reduction reactions.[23-27] Furthermore, its high V_{OC} can be directly applied to preparation of hydrogen by electrolysis of water, requiring 1.23 V.[28] Considering the overpotential of the water-splitting reaction, the V_{OC} of a photovoltaic cell needs to be higher than ~1.5 V.[29,30] From the energy diagram shown in Fig. 1, the maximum voltage of the $MAPbBr_3$-based HSC is estimated to be 1.6 V, suggesting that the hydrogen evolution from the electrolysis of water can be achieved in the future by a single $MAPbBr_3$-based HSC device without fabricating the tandem cell structures. Likewise,

promising applications are expected for the $MAPbBr_3$-based HSCs that exhibit ultrahigh V_{OC}.

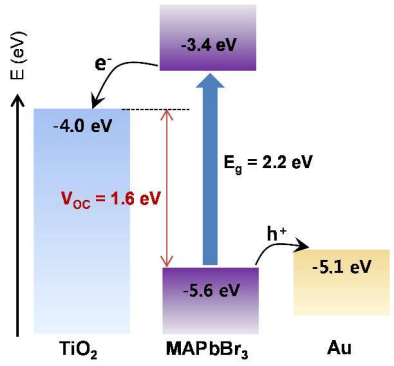

Fig. 1 Energy band diagram and charge separation principle for the $TiO_2/MAPbI_3/Au$ heterojunction solar cell (HSC).

Charge separation arising from the charge transfer in the $MAPbBr_3$-based HSC will be less efficient than that of conventional perovskite solar cells that employ HTMs to mediate the transfer of holes out of the valence band (VB) of light absorber. Concurrently, charge recombination inevitably occurs with a higher rate in the HSC devices, further degrading the photovoltaic properties such as short circuit current (J_{SC}) and V_{OC}. Therefore, charge transfer becomes more important in the HSC devices than the conventional perovskite solar cells. In this work, we controlled the interface between the $MAPbBr_3$ and the mesoporous TiO_2 layer in the $MAPbBr_3$ HSC. Interface control at TiO_2/perovskite or perovskite/HTM has often been attempted to improve charge transport efficiency in the perovskite solar cells.[31-34] Herein we found the coverage of the TiO_2 surface by a monolayer of carboxylate groups remarkably enhances photovoltaic performance of the $MAPbBr_3$ HSC. We also examined the effect of several types of carboxylate groups on the photovoltaic properties and measured the charge transfer efficiency and the electron lifetime in the mesoporous TiO_2 layer by applying time-resolved spectroscopic techniques.

Results and discussion

We introduced molecular carboxylates on the surface of mesoporous TiO_2 layer by dipping the film into the corresponding carboxylic acid solution. It is well known that the carboxylic acids have excellent binding affinity for TiO_2 surface.[35-39] For instance, in the dye-sensitized solar cells (DSSCs), various dye molecules with carboxylate terminal groups are stably anchored to the surface of mesoporous TiO_2 to form monolayer coverage.[37-39] The amounts of carboxylic acids adsorbed on the TiO_2 surface can be determined by monitoring the UV-visible absorption spectra, when the carboxylic acids exhibit characteristic absorption peaks. Previously, Arakawa et al. reported that density of carboxylic dyes adsorbed on the ~10 μm-thick mesoscopic TiO_2 film (derived from the ~20 nm-sized TiO_2 nanoparticle) are $1 - 2\times10^{-7}$ mol cm^{-2}.[37-39] In this work, we determined the density of phthalic acid (PA), exhibiting the characteristic absorption peak at ~280 nm, on the similar TiO_2 structure by the same technique. It was determined to be 2.2×10^{-7} mol cm^{-2}, which is compatible with the reported values of carboxylic dyes.[37-39]

SEM image for the cross-section of the $FTO/TiO_2/MAPbBr_3/Au$ is shown in Fig. 2a. The thickness of mesoporous TiO_2 layer is about 1.4 μm, and some of the spin-coated $MAPbBr_3$ seems to be infiltrated into the mesopores of the TiO_2 layer, but its major portion is overlay-coated on the top of TiO_2 surface by ~400 nm-thickness. As the back contact, Au layer was then deposited by vacuum evaporation technique with a thickness of ~60 nm. Magnified SEM image to the interfaces of $TiO_2/MAPbBr_3$ indicates that $MAPbBr_3$ is well-contacting the TiO_2 surface and also filling into TiO_2 mesopores. Nonetheless, there is a high possibility that TiO_2 surfaces located in the tiny pores are not completely covered with $MAPbBr_3$, due to difficulty of $MAPbBr_3$ infiltration. The cross-sectional SEM image for the bromoacetate (BAA)-treated device ($FTO/TiO_2/BAA/MAPbBr_3/Au$) is shown in Fig. 2b. By introducing BAA in the interface, $MAPbBr_3$ seems to be more tightly adhered to the TiO_2 surface, but the precise information to the extent of pore-filling into the TiO_2 pore structure could not be derived.

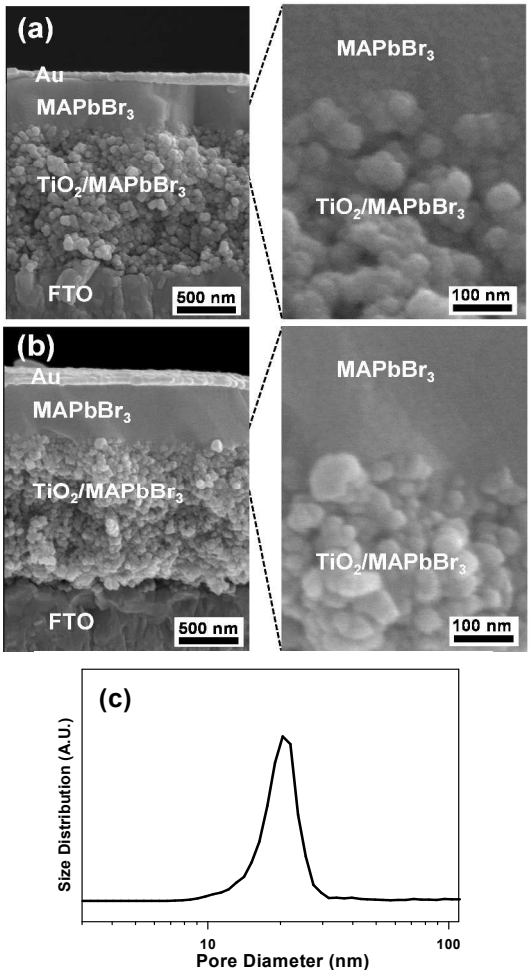

Fig. 2 Cross-sectional SEM images for $TiO_2/MAPbBr_3/Au$ (a) and $FTO/TiO_2/BAA/MAPbBr_3/Au$ (b) HSCs, and pore size distribution for the mesoporous TiO_2 layer derived from 20 nm-sized nanoparticle (c).

Pore size distributions in the fabricated mesoporous TiO_2 films were analyzed by N_2 adsorption–desorption isotherms. As shown in Fig. 2c, average pore diameter of the mesoporous TiO_2 film, derived from the 20 nm-sized nanoparticles, is ~21 nm, but the diameters of the generated pores are distributed from 8 to 30 nm. Considering that the pore-filling of $MAPbBr_3$ becomes difficult as the size of TiO_2 pore decreases, significant portion of TiO_2 surfaces, surrounding the narrow pores, would be exposed without deposition of $MAPbBr_3$. Then the uncovered TiO_2 surface could work as charge recombination site. That is, the uncovered TiO_2 surface would be gradually occupied with water species or hydroxyl groups present in the environment. Furthermore, its surface can be smeared by Au clusters during the deposition of Au CE. Accordingly, the electrons in the TiO_2 conduction band (CB), injected from the photo-excited $MAPbBr_3$, would be trapped on those sites, resultantly retarding the electron transport and then inducing the charge recombination from TiO_2 CB to $MAPbBr_3$ VB. Therefore, passivation of TiO_2 surface will be one of the key strategies to retard the charge recombination at the interface of $MAPbBr_3$ and TiO_2. In this work we introduced molecular carboxylates on the mesoporous TiO_2 surface. It is expected that small molecular carboxylic acids, typically less than 1 nm, can pave the entire TiO_2 surfaces, regardless of pore sizes. Logically, passivation process has to be performed after the deposition of $MAPbBr_3$ layer, but practically this process is difficult, because the coated $MAPbBr_3$ can be easily damaged during the deposition of carboxylic acid.

The carboxylate layer formed at the interface of $MAPbBr_3/TiO_2$ may not prevent the electron transport from $MAPbBr_3$ to TiO_2 CB, because it is a monolayer consisting of small molecular carboxylic acids. Moreover, the contact of $MAPbBr_3$ grains to TiO_2 surface can be improved by the presence of the molecular carboxylate layer through the chemical interaction of carboxylate terminal group and $MAPbBr_3$. In this regard, herein, we modified the surface of mesoporous TiO_2 layer with several carboxylic groups such as formic acid (FA), deoxycholic acid (DCA), phthalic acid (PA), acetic acid (AA), and bromoacetic acid (BAA), prior to the deposition of $MAPbBr_3$.

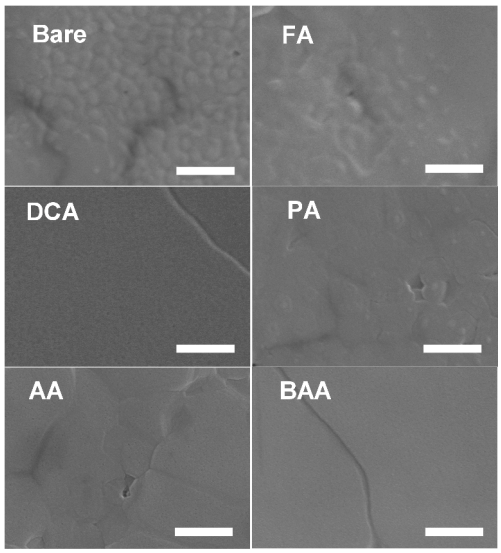

Fig. 3 Plan-view SEM images for the MAPbBr films deposited on the bare TiO_2, TiO_2/FA, TiO_2/DCA, TiO_2/PA, TiO_2/AA, and TiO_2/BAA. Each scale bar denotes 500 nm.

Plan-view SEM images of several $MAPbBr_3$ layers, deposited on the bare TiO_2 and the various carboxylate-treated TiO_2 films, are shown in Fig. 3. $MAPbBr_3$ film prepared on the bare TiO_2 layer does not show uniform morphology. Introduction of FA, which is the smallest carboxylic acid, slightly improves the uniformity of $MAPbBr_3$ film, but the introduction of bulky carboxylic acid such as DCA greatly improves the film uniformity, suggesting that the organic groups present on the TiO_2 surface provide a favorable environment in the growth of $MAPbBr_3$ grains. In addition, $MAPbBr_3$ film prepared on the AA or BAA-treated TiO_2 exhibits significantly improved surface morphology.

J-V curves were obtained from the several $MAPbBr_3$ HSCs, as shown in Fig. 4a. PCE of the HSC without surface modification (HSC-bare) was 2.65% with J_{SC} of 2.75 mA/cm^2, V_{OC} of 1.26 V, and *FF* of 0.76. By introducing several different carboxylate groups on the TiO_2 surface, photovoltaic properties of the devices were remarkably enhanced, as shown in Fig. 4a and in Table 1.

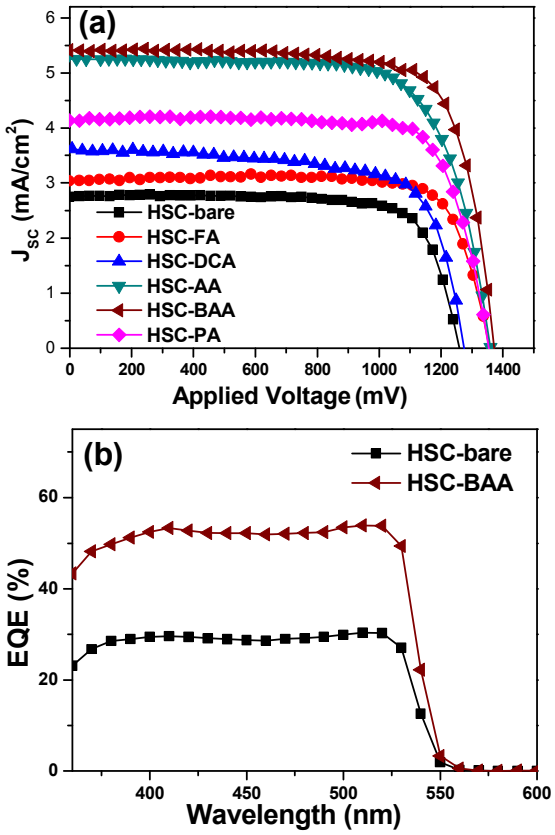

Fig. 4 (a) J-V curves several $MAPbI_3$ HSCs employing different carboxylic monolayers. (b) IPCE spectra of the bare $MAPbI_3$ HSC (HSC-bare), and the HSCs employing BAA (HSC-BAA).

It is also found that the enhancement of photovoltaic property is strongly dependent on the chemical structure of carboxylate groups. By introducing DCA with relatively bulky chain, the PCE of $MAPbBr_3$ HSCs was only slightly enhanced, with relatively lower *FF*. The acquired result suggests that bulky organic group located in the interface works as a dielectric layer, which seems to be detrimental for the electron transport from $MAPbBr_3$ to TiO_2. Contrarily, we found that the

smallest FA group is not effective either in enhancing the PCE of $MAPbBr_3$ HSC. The FA group seems to be too small to properly passivate the TiO_2 surface. Finally, by introducing carboxylate groups with medium-sized hydrocarbon chains such as PA, AA and BAA, photovoltaic properties of HSCs were enhanced significantly more. That is, not only J_{SC} but also V_{OC} was significantly increased, clearly indicating the efficient electron transport from $MAPbBr_3$ to TiO_2 layer as well as the suppression of charge recombination. Among them, the HSC devices with BAA (HSC-BAA) or AA (HSC-AA) exhibited relatively higher PCEs than those with PA (HSC-PA). In particular, HSC-BAA, exhibited the highest PCE of 5.57% with J_{SC} of 5.411 mA/cm^2, V_{OC} of 1.372 V, and *FF* of 0.75.

Table 1. Photovoltaic properties of the $MAPbI_3$ HSCs employing various carboxylic acids as interfacial layer.

Carboxylic acids for interface control	V_{OC} (mV)	J_{SC} (mA/cm^2)	FF (%)	PCE (%)
bare	1260	2.752	76.34	2.65±0.25
FA	1357	3.037	80.15	3.30
DCA	1274	3.616	67.46	3.11
PA	1355	4.135	78.76	4.41
AA	1365	5.366	70.15	5.18
BAA	1372	5.411	75.04	5.57±0.31

Notably, the obtained PCE approaches to that of the high performance $MAPbBr_3$ perovskite cell employing spiro-OMETAD as HTM (PCE = 6.7%).[20] The obtained results suggest that the enhanced PCE is closely related with the interaction affinity of alkyl chain part of carboxylic acid, facing to the $MAPbBr_3$. That is, bromoacetate group in the BAA seems to have an intimate interaction with $MAPbBr_3$, because the Br group can be used to connect with $MAPbBr_3$, as described in Fig. 5. Relatively lower PCE of HSC-PA utilizing phthalic acid can be attributed to weaker chemical interaction between phenyl group and $MAPbBr_3$.

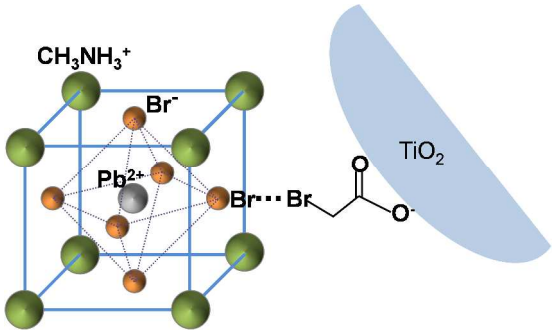

Fig. 5 A proposed schematic diagram describing the role of interfacial BAA group in connecting TiO_2 and $MAPbBr_3$.

The incident photon to current conversion efficiency (IPCE) spectra of the bare $MAPbBr_3$ HSC and the HSCs employing BAA are shown in Fig. 4b. The integrated current densities estimated from the IPCE spectra are in good agreement with the J_{SC} values acquired from the J-V curves. Overall external quantum efficiency (EQE) was enhanced approximately twice by introducing BAA group, but the EQE edge of the HSC devices was not altered, suggesting that the band structure of $MAPbBr_3$ was not influenced by the introduced BAA group on the TiO_2 surface.

To examine the role of passivation in the photovoltaic performance of $MAPbBr_3$ HSCs, we measured time-resolved photoluminescence (PL) of solar cells containing various carboxylic acid layers. In principle, by comparing PL lifetimes of the bare $MAPbBr_3$ film and the $MAPbBr_3/TiO_2$ bilayer films (with or without a carboxyl acid monolayer), we can characterize the dynamics and the efficiency of electron transfer across the interface. As can be seen in Fig. 6 and Table 2, the bare $MAPbBr_3$ film exhibits the PL decay with the time constant of τ_P = 86.5 ± 2.5 ns. The addition of the TiO_2 electron-quenching layer accelerates the PL decay substantially, resulting in the PL decay with the time constant of $\tau_{interface}$ = 8.9 ± 0.2 ns for the $MAPbBr_3/TiO_2$ bilayer film. Considering that the accelerated PL quenching in the bilayer film arises from electron transfer across the interface, we can obtain the relation of $1/\tau_{interface} = 1/\tau_P + 1/\tau_{CT}$, from which we estimated the charge transfer time of τ_{CT} = 9.9 ns and the charge transfer efficiency (CTE = $k_{CT}/k_{interface} = \tau_{interface}/\tau_{CT}$) of 89.7 %. In overall the PL lifetime decreases significantly when adding a carboxyl acid monolayer between $MAPbBr_3$ and TiO_2. For TiO_2/FA/$MAPbBr_3$ film, PL lifetime of $\tau_{interface}$ was virtually the same as that of bare $TiO_2/MAPbBr_3$, suggesting that that FA is too small carboxylate to passivate the TiO_2 surface. PL lifetimes of $\tau_{interface}$ for the carboxylate-treated devices decrease in the order of DCA<PA<AA<BAA, indicating that BAA is the most suitable interfacial layer in expediting the charge injection from $MAPbBr_3$ to TiO_2. Subsequently, we estimated τ_{CT} and CTE for the $MAPbBr_3/TiO_2$ films passivated with various carboxylates. The trend of τ_{CT} was the same as that of $\tau_{interface}$, whereas the CTEs of the HJSs were varied in the order of FA>DCA>PA>AA>BAA. In overall, the obtained result is in good agreement with the trend of photovoltaic efficiency except FA-treated sample.

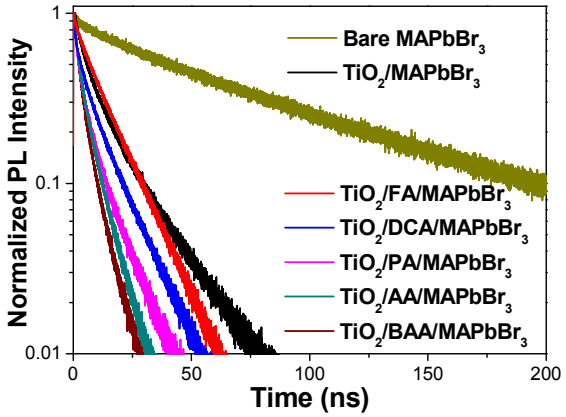

Fig. 6. PL decays of bare $MAPbBr_3$, $TiO_2/MAPbBr_3$, various TiO_2/carboxylic acid/$MAPbBr_3$ samples. It is clearly seen that the PL decay is accelerated with the addition of carboxylate layers. The time resolution of the time-resolved PL measurements was ~190 ps.

The decrease of τ_{CT} and the improved CTE with the addition of passivation layer indicate that the presence of a passivation layer improves charge injection into TiO_2 and ultimately leads to the increase of PCE. In particular, passivation with the BAA

monolayer gives the highest CTE and PCE, reflecting the subtle influence of the molecular structure of passivating molecules on the photovoltaic performance. Specifically, the BAA molecule can interact favorably with $MAPbBr_3$ and TiO_2 via a Br atom and a carboxylate group, respectively, to strengthen the chemical linkage between $MAPbBr_3$ and TiO_2 materials, as schematically proposed in Fig. 5. This proposed scheme is supported by the SEM image shown in Fig. 3 where we can see that the $MAPbBr_3$ film is grown more uniformly on the surface of BAA/TiO_2.

Table 2. Charge transfer times and efficiencies estimated from PL lifetimes of $MAPbBr_3$ HSCs employing various carboxylic acids as interfacial layer.

Samples	$\tau_{interface}$ (or τ_P) (ns)	τ_{CT} (ns)	CTE (%)
$MAPbBr_3$	86.5 ± 2.5	--	--
$TiO_2/MAPbBr_3$	8.9 ± 0.2	9.9	89.7
$TiO_2/FA/MAPbBr_3$	10.1 ± 0.2	11.4	88.3
$TiO_2/DCA/MAPbBr_3$	7.2 ± 0.2	7.9	91.6
$TiO_2/PA/MAPbBr_3$	4.6 ± 0.1	4.9	94.6
$TiO_2/AA/MAPbBr_3$	4.3 ± 0.1	4.5	95.0
$TiO_2/BAA/MAPbBr_3$	3.5 ± 0.1	3.7	95.9

In addition, to determine the lifetime of photogenerated electrons, we performed the pulsed light-induced transient measurements (PLITM) of photocurrent analysis for FTO/TiO_2/$MAPbBr_3$/Au devices with or without a carboxylate monolayers. The electron lifetime (τ_e) was determined by fitting the decay of a transient photocurrent with $\exp(-t/\tau_e)$,[40-43] as shown in Fig. 7.

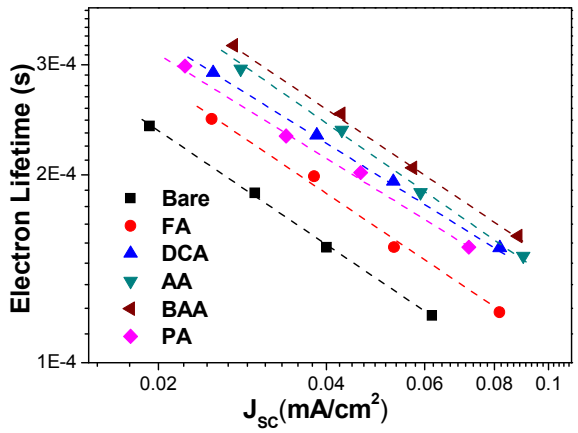

Fig. 7 Electron lifetime (□$_e$) vs. J_{SC} for the bare $MAPbI_3$ HSC and the HSCs employing various carboxylic acids.

The τ_e value, measured under the open-circuit condition, represents the portion of electrons that survive the recombination from TiO_2 CB to perovskite VB or Au CE. We found that τ_e values significantly increased by introducing carboxylate monolayers on the TiO_2 surfaces. This can be rationalized that electron-hole recombination at the interface of $TiO_2/MAPbBr_3$ can be reduced by the presence of carboxylate monolayer, because the carboxylate groups block the direct contact between TiO_2 and Au CE or the adsorption of water species onto TiO_2 surface. In overall, τ_e values for the carboxylate-treated devices increase in the order of FA<PA<DCA<AA<BAA, as shown in Fig. 7. Notably, DCA-treated TiO_2 showed relatively larger τ_e value, comparing with its low PCE, suggesting that bulky DCA group is rather effective in blocking the electron-hole recombination. BAA-treated TiO_2 exhibits significantly larger τ_e value, indicating that it is the most suitable carboxylate in reducing the electron-hole recombination.

To summarize, we demonstrated that the introduction of molecular carboxylate groups at the interface of $TiO_2/MAPbBr_3$ expedites the electron injection from $MAPbBr_3$ to TiO_2 CB and also suppresses the charge recombination of the injected electrons in the TiO_2 CB. Among the carboxylic acids used for the interface control, DCA is the largest, whereas formic acid (FA) is the smallest. Both are not efficient in enhancing photovoltaic property of HJS. DCA is too large and FA is too small to play an appropriate role as interfacial layer. We found that acetic acid or its derivative is more adequate as interfacial layer. Particularly, it was found that bromoacetic acid (BAA) is the most suitable carboxylate, because BAA interfacial layer can help the tight binding of perovskite layer onto TiO_2 alyer by the role of Br group. As demonstrated, the control of the $TiO_2/MAPbBr_3$ interface is crucial for enhancing the photovoltaic performance of $MAPbBr_3$-based HSC.

Experimental

Synthesis of $MAPbBr_3$

$MAPbBr_3$, used as light absorber, was prepared according to the following procedure. A 0.294 mol hydrobromic acid (48 wt % in water, Aldrich) and 0.098 mol methylamine (40 wt % in methanol, TCI) were mixed and stirred in an ice bath for 2 h. The solvent in this mixture was completely evaporated at 60 °C to obtain the $CH_3NH_3Br{\cdot}2HBr$ precipitate. The collected $CH_3NH_3Br{\cdot}2HBr$ powder was washed several times by diethyl ether. For further purification, $CH_3NH_3Br{\cdot}2HBr$ was redissolved in 30 mL ethanol (Aldrich) and subsequently recrystallized by adding excess diethyl ether. To prepare $CH_3NH_3PbBr_3$, the prepared 0.411 g $CH_3NH_3Br{\cdot}2HBr$ and 0.569 g lead acetate (99%, Aldrich) were dissolved in 1.0 mL DMF with stirring at 60 °C for 1 h. The obtained viscous solution was then cooled to room temperature, and filtered by a syringe filter (pore size 0.45 μm, Whatman) to remove impurities.

Solar cell fabrication

A buffer layer with a ~20 nm-thickness was prepared by spin-coating of the 0.15 M titanium (IV) bis(ethylacetoacetato) diisopropoxide solution in 1-butanol on a FTO glass (Pilkington, TEC-7, 7 Ω/sq), followed by annealing at 500 °C for 30 min. Over the buffer layer, mesporous TiO_2 layer was deposited using a commercial paste (DyeSol, DSL 18NR-T), which was pre-diluted to 1/3 by adding ethanol. The prepared TiO_2 paste was spin-coated at 2000 rpm for 30 s and then annealed at 500 °C for 30 min.

To form carboxylate monolayer on the surface of mesoporous TiO_2, the prepared TiO_2 substrate was dipped into the ethanol solution containing 0.010 M carboxylic acid. After the dipping for 1 h, the mesoporous TiO_2 substrate was washed thoroughly by ethanol to remove physically absorbed carboxylic acids. The surface modified mesoporous TiO_2 films were then used to deposit $MAPbBr_3$ layer by spin-coating method. That is, 0.15 mL of 1.5 M $MAPbBr_3$ in DMF solution was dropped on the 2 cm × 2 cm substrate. After holding for 60

s, the substrate was then spun at 1000 rpm for 30 s. Au layer with a thickness of 60 nm was deposited by thermal evaporator (Korea Vacuum Tech.) to form the counter electrode (CE). The active area of the device was defined by a metal mask with a size of 0.122 cm^2.

Characterization

To determine the amounts of carboxylic acids adsorbed on the TiO_2 surface, PA-adsorbed TiO_2 sample was employed, because PA shows a characteristic absorption peak at ~280 nm. The PA-adsorbed mesoscopic TiO_2 film (size: 3×3 cm^2, thickness: 10 μm) prepared from 20 nm-sized TiO_2 NP was immersed in 10 ml of 3×10^{-4} M NaOH in a mixed solvent (water/ethanol = 1:1, v/v) for 4 h to completely desorb the PA as sodium phthalate. By measuring the absorbance of sodium phthalate at 280 nm by UV-visible absorption spectroscopy, the absorbed amount of PA was determined.

The morphologies of the deposited $MAPbBr_3$ films and the fabricated HJSs were examined by field-emission scanning electron microscopy (SEM, Hitachi S4300). Photocurrent–voltage (I–V) measurements were performed using a Keithley model 2400 source measurement unit. A 300 W Xenon lamp (Spectra-Physics) was used as the light source and the light intensity was adjusted using an NREL-calibrated Si solar cell equipped with a KG-5 filter for approximating AM 1.5 G one sunlight intensity. The magnitude of the alternate signal was 10 mV. The incident photon to current efficiency (IPCE) spectra was measured as a function of wavelength from 350 to 850 nm using a specially designed IPCE system (PV Measurements, Inc.).

Time-resolved spectroscopies

Time-resolved photoluminescence (PL) was measured using time-correlated single photon counting (TCSPC) spectrometer (FluoTime 200, PicoQuant). Film samples were illuminated by ~100 ps laser pulses of 390 nm center wavelength through FTO glass, and the emission from $CH_3NH_3PbBr_3$ was collected at the wavelength of 540 nm at 90˚ angle with respect to the incidence of excitation light. The temporal resolution of time-resolved PL measurements was ~190 ps. The PL decays of all the samples were best fit by a sum of two exponentials, $A_1 \exp(-t/\tau_1) + A_2 \exp(-t/\tau_2)$. The multi-exponential PL decay can be attributed to structural heterogeneity of film samples. To simplify the comparison between PL decays of various samples, we approximated the PL decay by a single exponential of an amplitude-weighted average lifetime, $\tau_{avg} = A_1\tau_1 + A_2\tau_2$.

The electron life time (τ_e) in the TiO_2 CB was measured by a home-made PLITM of photocurrent and voltage equipment.[40-43] To obtain transient photocurrent, the laser pulse (λ = 532 nm, pulse duration 7 ns, Laser-Export Co. Ltd. Model: LCS-DTL-314QT) was irradiated from the counter electrode (Au) side of $MAPbI_3$ HSC, while the bias light (470 nm wavelength LED lamp, Asahi Inc.) was illuminated from the working electrode (FTO) side. The measurement was implemented at the open-circuit condition and the measurements were repeated while the intensity of the bias light being varied.

Conclusions

Molecular carboxylate monolayers introduced at the interface of $MAPbBr_3$ and TiO_2 remarkably enhances the photovoltaic properties of $MAPbBr_3$–based HSCs. In particular, the presence of a BAA monolayer at the $TiO_2/MAPbBr_3$ interface remarkably increases PCE from 2.65 % (no passivation layer) to 5.62 % (with a BAA passivation layer) with J_{SC} of 5.62 mA/cm^2, V_{OC} of 1.37 V, and *FF* of 0.75. The time-resolved PL and the pulsed light-induced transient measurements of photocurrent and voltage analyses indicate that the interfacial monolayer induces faster electron injection from the $MAPbBr_3$ to TiO_2 layer and the suppression of charge recombination. To account for these findings, we propose that the carboxyl acid monolayer strengthens the chemical linkage between $MAPbBr_3$ and TiO_2 materials as well as isolates TiO_2 from Au CE.

Acknowledgements

This work was supported by the Korea Center for Artificial Photosynthesis (KCAP) located in Sogang University funded by the Minister of Science, ICT and Future Planning (MSIP) through the National Research Foundation of Korea (No. 2009-0093884)".

Notes and references

[a]*Department of Chemistry and Chemical Engineering, Inha University, Incheon 402-751, Korea. E-mail: wanin@inha.ac.kr; Tel:+82-32-863-1026*
[b]*Department of Chemistry and Chemical Engineering, Inha University, Incheon 402-751, Korea. E-mail: jkim5@inha.ac.kr; Tel:+82-32-860-7678*

1 H.-S. Kim, C.-R. Lee, J.-H. Im, K.-B. Lee, T. Moehl, A. Marchioro, S.-J. Moon, R. Humphry-Baker, J.-H. Yum, J. E. Moser, M. Grätzel and N.-G. park, *Sci. Rep.*, 2012, **2**, 591.
2 M. M. Lee, J. Teuscher, T. Miyasaka, T. N. Murakami and H. J. Snaith, *Science*, 2012, **338**, 643–647.
3 J.-H. Im, I.-H. Jang, N. Pellet, M. Grätzel and N.-G. Park, *Nature Nanotech.*, 2014, **9**, 927–932.
4 H. Zhou, Q. Chen, G. Li, S. Luo, T.-B. Song, H.-S. Duan, Z. Hong, J. You, Y. Liu and Y. Yang, *Science*, 2014, **345**, 542–546.
5 N. J. Jeon, J. H. Noh, Y. C. Kim, W. S. Yang, S. Ryu and S. I. Seok, *Nature Mater.*, 2014, **13**, 897–903.
6 A. G. Pattantyus-Abraham, I. J. Kramer, A. R. Barkhouse, X. Wang, G. Konstantatos, R. Debnath, L. Levina, I. Raabe, M. K. Nazeeruddin, M. Gratzel and E. H. Sargent, *ACS Nano*, 2010, **4**, 3374–3380.
7 D. A. R. Barkhouse, R. Debnath, I. J. Kramer, D. Zhitomirsky, A. G. Pattantyus-Abraham, L. Levina, L. Etgar, M. Grätzel and E. H. Sargent, *Adv. Mater.*, 2011, **23**, 3134–3138.
8 B. Ding, Y. Wang, P.-S. Huang, D. H. Waldeck and J.-K. Lee, *J. Phys. Chem. C*, 2014, **118**, 14749–14758.
9 L. Etgar, P. Gao, Z. Xue, Q. Peng, A. K. Chandiran, B. Liu, M. K. Nazeeruddin and M. Gratzel, *J. Am. Chem. Soc.*, 2012, **134**, 17396–17399.
10 Z. Ku, Y. Rong, M. Xu, T. Liu and H. Han, *Sci. Rep.,* 2013, 3, 3132.
11 Y. Yang, J. Xiao, H. Wei, L. Zhu, D. Li, Y. Luo, H. Wu and Q. Meng, *RSC Adv.*, 2014, **4**, 52825–52830.
12 S. Aharon, S. Gamliel, B. E. Cohen and L. Etgar, *Phys. Chem. Chem. Phys.*, 2014, **16**, 10512–10518.
13 W. A. Laban and L. Etgar, *Energy Environ. Sci.*, 2013, 6, 3249–3253.
14 J. Shi, J. Dong, S. Lv, Y. Xu, L. Zhu, J. Xiao, X. Xu, H. Wu, D. Li, Y. Luo and Q. Meng, *Appl. Phys. Lett.*, 2014, **104**, 063901–4.
15 B. Peng, G. Jungmann, C. Jager, D. Haarer, H.-W. Schmidt and M. Thelakkat, *Coord. Chem. Rev.*, 2004, **248**, 1479–1489.
16 N.-G. Park, *J. Phys. Chem. Lett.*, 2013, 4, 2423–2439.
17 A. Dymshits, A. Rotem and L. Etgar, *J. Mater. Chem. A*, 2014, **2**, 20776–20781.
18 Y. Zhao, A. M. Nardes and K. Zhu, *Faraday Discuss.*, 2014, DOI:10.1039/C4FD00128A.
19 K. Kakiage, T. Kyomen and M. Hanaya, *Chem. Lett.*, 2013, **42**, 1520–1521.
20 S. Ryu, J. H. Noh, N. J. Jeon, Y. C. Kim, W. S. Yang, J. Seo and S. I. Seok, *Energy Environ. Sci.*, 2014, **7**, 2614–2618.
21 E. Edri, S. Kirmayer, M. Kulbak, G. Hodes and D. Cahen, *J. Phys. Chem. Lett.*, 2014, **5**, 429–433.

22 F. C. Janusch, E. Wiesenmayer, E. Mankel, A. Binek, P. Angloher, C. Fraunhofer, N. Giesbrecht, J. M. Feckl, W. Jaegermann, D. Johrendt, T. Bein and P. Docampo, *J. Phys. Chem. Lett.*, 2014, **5**, 2791–2795.
23 J. A. Turner, *Science*, 2004, **305**, 972–974.
24 A. Heller, *Acc. Chem. Res.* 1981, **14**, 154–162.
25 M. G. Walter, E. L. Warren, J. R. McKone, S. W. Boettcher, Q. Mi, E. A. Santori, and N. S. Lewis, *Chem. Rev.*, 2010, 110, 6446–6473.
26 M. Grätzel, *Nature*, 2001, **414**, 338–344.
27 J.-W. Jang, S. Cho, G. Magesh, Y. J. Jang, J. Y. Kim, W. Y. Kim, J. K. Seo, S. Kim, K.-H. Lee and J. S. Lee, *Angew. Chem. Int. Ed.,* 2014, **53**, 5852 –5857.
28 J. Luo, J.-H. Im, M. T. Mayer, M. Schreier, M. K. Nazeeruddin, N.-G. Park, S. D. Tilley, H. J. Fan and M. Grätzel, *Science*, 2014, **345**, 1593–1596.
29 K. Zeng and D. Zhang, *Prog. Energy Combust. Sci.,* 2010, **36**, 307–326.
30 R. N. Singh, D. Mishra, Anindita, A. S. K. Sinha and A. Singh, *Electrochem. Commun.,* 2007, **9**, 1369–1373.
31 A. Abrusci, S. D. Stranks, P. Docampo, H.-L. Yip, A. K.-Y. Jen and H. J. Snaith, *Nano Lett.*, 2013, **13**, 3124–3128.
32 K. Wojciechowski, S. D. Stranks, A. Abate, G. Sadoughi, A. Sadhanala, N. Kopidakis, G. Rumbles, C.-Z. Li, R. H. Friend, A. K.-Y. Jen and H. J. Snaith, *ACS Nano*, 2014, DOI: 10.1021/nn505723h.
33 Y. Ogomi, A. Morita, S. Tsukamoto, T. Saitho, Q. Shen, T. Toyoda, K. Yoshino, S. S. Pandey, T. Ma and S. Hayase, *J. Phys. Chem. C*, 2014, **118**, 16651–16659.
34 A. Abate, M. Saliba, D. J. Hollman, S. D. Stranks, K. Wojciechowski, R. Avolio, G. Grancini, A. Petrozza and H. J. Snaith, *Nano Lett.*, 2014, **14**, 3247–3254.
35 C.-Y. Wang, H. Groenzin and M. J. Shultz, *J. Am. Chem. Soc.*, 2005, **127**, 9736-9744.
36 X.-Q. Gong, A. Selloni and A. Vittadini, *J. Phys. Chem. B,* 2006, **110**, 2804-2811.
37 K. Hara, K. Sayama, Y. Ohga, A. Shinpo, S. Suga and H. Arakawa, Chem. Commun., 2001, 569-570.
38 K. Hara, Y. Dan-oh, C. Kasada, Y. Ohga, A. Shinpo, S. Suga, K. Sayama and H. Arakawa, Lngmuir, 2004, 20, 4250-4210.
39 Z.-S. Wang, H. Kawauchi, T. Kashima and H. Arakawa, Coord. Chem. Rev., 2004, 248 1381-1389.
40 J. van de Lagemaat and A. J. Frank, *J. Phys. Chem. B,* 2001, ***105***, 11194-11205.
41 S. Takenaka, Y. Maehara, H. Imai, M. Yoshikawa and S. Shiratori, *Thin Solid Films*, 2003, **438**, 346-351.
42 Q. Wang, J. Moser and M. Grätzel, *J. Phys. Chem. B*, 2005, **109**,14945-14953.
43 J.-W. Lee, T.-Y. Lee, P. J. Yoo, M. Grätzel, S. Mhaisalkar and N.-G. Park, J. Mater. Chem. A, 2014, **2**, 9251-9259.

Journal of Materials Chemistry A RSCPublishing

ARTICLE

Graphical Abstract

Enhancement of photovoltaic properties of $CH_3NH_3PbBr_3$ heterojunction solar cells by modifying mesoporous TiO_2 surface with carboxyl groups

Hyun Bin Kim, Iseul Im, Yeomin Yoon, Sang Do Sung, Eunji Kim, Jeongho Kim and Wan In Lee

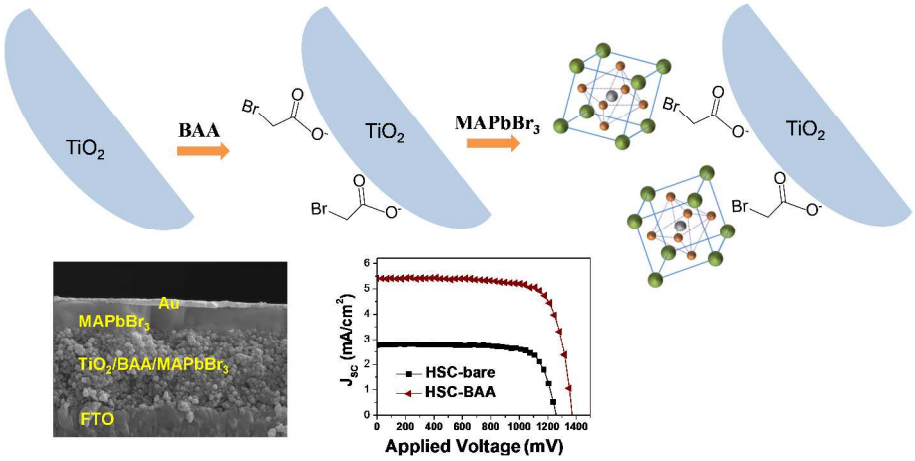

In a novel heterojunction solar cell employing $CH_3NH_3PbBr_3$ ($MAPbBr_3$) as light absorber, the introduction of a carboxylate monolayer on the mesoporous TiO_2 surfaces significantly enhances J_{SC} as well as V_{OC}.